NEW EVIDENCE FOR A RELATION BETWEEN WIND STRESS AND WAVE AGE FROM MEASUREMENTS DURING ASGAMAGE

W. A. OOST, G. J. KOMEN, C. M. J. JACOBS and C. VAN OORT
Royal Netherlands Meteorological Institute (KNMI), the Netherlands

(Received in final form 17 August 2001)

Abstract. Data from the 1996 ASGAMAGE* experiment, performed in the southern North Sea at research platform Meetpost Noordwijk (MPN), are analysed for the parameters affecting the momentum flux. The stress turns out to be quadratically related to the 10-m wind speed and linearly to the wind speed at a wavelength related level. The Charnock parameter (dimensionless roughness length) shows a pronounced correlation with wave age. This implies, due to a coupling between wave age and the steepness of the waves, a connection between the stress and the steepness. We find that our North Sea results are consistent with open ocean observations. For a given wind speed the mean stress at MPN turns out to be higher because the wave age there is in general lower. We define and give an expression for a drag coefficient at a wavelength related level that can be calculated straightforwardly from the wave age and then reduced to a standard level.

Keywords: Air-sea interaction, Charnock parameter, Drag coefficient, Momentum flux, Wave field.

1. Introduction

Both over sea and over land the vertical transport of momentum is of paramount importance in studies of the atmospheric surface layer, weather and climate. In model studies the momentum flux, τ is generally computed from the so-called bulk formulation in which τ is written as

$$\tau = \rho_a C_D (U_a - U_s)^2$$

with U_a the wind speed at a chosen level and U_s the wind speed at a level close to the surface, taken to be the roughness length, z_0. At sea, z_0 is defined as the level where the wind speed, extrapolated downwards using a logarithmic wind profile, is equal to the speed of the water surface. The proportionality coefficient, the drag coefficient C_D, can be determined in experiments in which the momentum flux is measured and related to the wind speed. Despite many years of experimental

* ASGAMAGE is a contraction of ASGASEX and MAGE. ASGASEX (Air Sea GAS EXchange) is a series of experiments aimed at measuring and interpreting the transport of CO_2 between air and sea; MAGE (Marine Aerosol and Gas Exchange) is Activity 1.2. of the International Global Atmospheric Chemistry (IGAC) project of IGBP, the International Geosphere Biosphere Programme of the United Nations.

studies the accuracy with which C_D is presently known is still very limited, especially over the sea, where for every wind speed there is a range of values of this coefficient, resulting from various experiments. The uncertainty is roughly a factor of 2. The question is whether and how this spread can be reduced. In this paper, we will investigate the role of the underlying wave field in this connection.

There is a long history of research into this subject, and an ongoing debate about the presence of a noticeable effect of the wave field on C_D. Well known in this connection is the 1986 HEXMAX campaign, the HEXOS Main Experiment (Smith et al., 1992), which took place at and around research platform Meetpost Noordwijk (MPN, Figure 1), 9 km off the Dutch coast, the same place where the data of this study originated. HEXMAX provided the basic material for a number of publications about the relationship between the momentum flux and the wave field (Smith et al., 1992; Maat et al., 1991; Janssen, 1997; Oost, 1998). All of these publications were concerned with the relation of the drag coefficient C_D and the wave-age parameter $\xi = c_p u_*^{-1}$ (with c_p the phase velocity of the peak of the wave spectrum and u_* the friction velocity), which for wind sea can be interpreted as a measure for the stage of development of the wave field (see e.g., Donelan et al., 1993; and Komen et al., 1997 for reviews). Doubts still remained about the applicability of the relationships found, however, both on theoretical (Makin et al., 1995) and experimental (Smith, 1980, further indicated as S80, Yelland and Taylor, 1996; Yelland et al., 1998) grounds. These doubts are largely based on the observation that, for a given wind speed, stress measurements in the open ocean are systematically lower than those found during HEXMAX. The fact that MPN is standing in tidal waters with a depth of, on average, 18 m, where sufficiently long waves could be feeling the bottom, has been noted as a possible cause of this difference (Oost, 1998).

In the present study we will use momentum flux measurements, made during the 1996 ASGAMAGE experiment, an air-sea gas exchange study in which 14 institutes from seven countries, among them KNMI, participated. ASGAMAGE took place, like HEXMAX, at and around MPN. For comparison with deep water measurements we will primarily use data from S80, because this paper contains more wave information than Yelland et al. (1998), and furthermore the S80 data were obtained with the eddy correlation method, the same technique we used during ASGAMAGE. On average the Yelland et al. (1998) and the S80 stress values are anyway very similar. The use of the inertial-dissipation method, in combination with the uncertainty in the so-called imbalance term, crucial for this technique, made us refrain from a comparison with the data of Eymard et al. (1999). Furthermore, the latter data were not corrected for flow distortion, which might have affected the reported fluxes significantly.

The ASGAMAGE data set is in most respects superior to that of HEXMAX. Improvements consist of better data handling and recording, the availability of directional wave measurements, a much larger number of data runs, higher instrument accuracies and an extended range of atmospheric stabilities: HEXMAX covered a single measurement period in the fall of 1986 with a permanently unstable atmosphere, whereas ASGAMAGE comprised two measurement periods, one in the spring (the 'A'-period) with mainly stable, and one in the fall (the 'B' period) with predominantly unstable stratification. In contrast HEXMAX was superior to ASGAMAGE in one aspect, viz. the maximum wind speed.

In the present paper we will try to resolve some questions about the wave age dependence of the stress and the representativity of momentum exchange experiments in the southern North Sea. We will show that this difference can be explained as a consequence of the longer fetches generally met in the open ocean.

In the next section we will present the formalism we have used in our interpretation. Because we are looking for fairly subtle effects, we will have to be very sure that we are dealing with correct values. In Section 3 we will therefore discuss at some length how the data were obtained and estimate the size of a number of disturbing effects that might have affected them. In Section 4 we will first look for the optimal standard level for wind speed, then into relationships between stress, wind speed and the properties of the wave field, compare our results with those from the open ocean and finally propose a relationship for a drag coefficient at a wavelength related level. In Section 5 we present our overall conclusions.

2. Theory

The wind speed $U(z)$ over sea, the way we will use it, is given by

$$U(z) = U_m(z) - U_c \tag{1}$$

with $U_m(z)$ the wind speed measured at some height z above the mean sea level and U_c the surface current component in the wind direction. For $U(z)$ we assume the stability corrected logarithmic wind profile of the Monin–Obukhov similarity theory (Monin and Obukhov, 1954)

$$U(z) = \frac{u_*}{\kappa}\left[\ln\left(\frac{z}{z_0}\right) - \Psi_m\left(\frac{z}{L}\right)\right], \tag{2}$$

where u_* is the friction velocity, defined as the square root of the (kinematic) turbulent stress $\tau = -\langle u'w'\rangle$, with u' and w' the fluctuations in the along-wind and vertical wind components. z_0 is the roughness length (the height at which under neutral conditions the value of $U(z)$, extrapolated to the surface, is 0) and $\Psi_m(zL^{-1})$ the stability correction function for momentum, with L the Obukhov length. $z = 0$ denotes the mean water surface and κ is the von Kármán constant (κ = 0.4). For $\Psi_m(zL^{-1})$ we use the Businger–Dyer stability functions (Businger et al., 1971; Dyer and Hicks, 1970), as integrated by Paulson (1970); his expressions can be found in many text books.

A common way to non-dimensionalise z_0 is due to Charnock (1955) who wrote

$$z_0 = \alpha \frac{u_*^2}{g} \tag{3}$$

with g the acceleration of gravity (for which we used 9.81 ms^{-2}). The non-dimensional roughness α is called the Charnock parameter. To remove the (generally small over the sea) effects of different stabilities from our treatment we define the wind speed reduced to neutral circumstances as

$$U_N(z) = \frac{u_*}{\kappa} \ln\left(\frac{z}{z_0}\right) = \frac{u_*}{\kappa} \ln\left(\frac{gz}{\alpha u_*^2}\right). \tag{4}$$

We calculated L from our measured data as:

$$L = \frac{-\theta_v u_*^3}{g\kappa \langle w'\theta_w' \rangle}$$

with θ_v the potential virtual temperature and primes as before denoting fluctuating parts. L, or, better, zL^{-1} was then used to compute the 10-m neutral wind speed $U_N(10)$ (also indicated as U_{N10}). The 10-m drag coefficient C_{D10}, defined by

$$\tau = C_{D10} U^2(10) \tag{5}$$

can be determined from measurements of $U(10)$ and u_*. Its precise value again depends on the atmospheric stability. We therefore use the neutral 10-m drag coefficient C_{DN10} defined as

$$\tau = C_{DN10} U_N^2(10). \tag{6}$$

In experiments at sea one measures the mean wind speed at a particular height, air and water temperature, humidity, the fluxes of momentum, heat and moisture and the surface current. Application of the foregoing formalism then allows α to be determined. In practice it is more convenient to work with either $\ln(\alpha)$ or C_{DN10} which are related by

$$C_{DN10}^{1/2} = \frac{\kappa}{\ln\left(\frac{10g}{u_*^2}\right) - \ln(\alpha)}. \tag{7}$$

Global and regional general circulation models often use Equations (1) and (4) to relate the surface stress to the wind speed at the lowest level. The choice of α then determines the value of the stress. This underlines the importance of its experimental and theoretical determination.

The basic quantity we need, to find out about an effect of the waves on the stress, is the ratio of the wave induced stress τ_w and the total stress τ. However, $\tau_w\tau^{-1}$ is not available for experimental verification. The wave age $\xi = c_p u_*^{-1}$ is generally used as a proxy for $\tau_w\tau^{-1}$ and the question of the effect of the waves on the stress can then be rephrased as: Does the Charnock parameter α depend on ξ, and, if so, how?

We follow the convention to formulate the wave-age dependence of α as a power law

$$\alpha = \mu(\xi)^n, \tag{8}$$

so μ and n are then determined from a plot of $\ln(\alpha)$ versus $\ln(\xi)$.

3. The Data

3.1. Data characteristics and data handling

MPN is standing in tidal waters with an average depth of 18 m, at a position 9 km. off the Dutch coast (Figure 1). It is a bottom mounted and therefore very stable platform, allowing precise determination of notably the vertical wind component, which is notoriously difficult to measure on a moving platform like a ship or a buoy. This makes it possible to do eddy correlation measurements at sea over water with an appreciable depth. The instruments for those measurements are mounted at the end of a 21-m long boom, extending from the west side of the platform. An outrigger of this length, which is just as necessary, but not feasible on a ship, is sufficient to reduce flow distortion due to the platform body to an acceptable level (Wills, 1984; Oost et al., 1994). During ASGAMAGE the instruments used to determine the momentum flux were a three-component Gill (Solent) ultrasonic anemometer, type R2A, and a pressure anemometer (PA), an instrument developed at KNMI (Oost et al., 1991). Due to technical problems the number of PA data was severely limited and we have only used wind data from the sonic anemometer in what follows. On those occasions where data from both instruments were available they did agree as well as could be expected from two instruments with their sensor heads at around 4 m (for the PA), and 6 m (for the sonic) above the mean water level. Data were sampled with a frequency of 40 Hz, allowing analysis to 20 Hz. The length of a full run was some 55 min (3277 s, corresponding to 2^{17} samples). Only runs with wind directions in the range 200°–270°–360° (SSW to N over W) were accepted, again to prevent flow distortion effects. Each 55-min run was later divided into three 18-min (1092.25 s) sections, which are the runs we will use in this paper. In this way we could increase the number of independent flux determinations without sacrificing accuracy (the low frequency variability of the 18-min runs was not higher than that of the long ones). Mean wind speeds were taken relative to the tidal current, calculated with the WAQUA model (Gerritsen et

Figure 1. Research platform Meetpost Noordwijk (MPN). The platform is situated 9 km off the Dutch coast in (on average) 18 m deep water.

al., 1981). The total number of 18-min runs was 890, 330 in the spring period and 560 in the fall.

The neutral wind speed at a height of 10 m (Equation (4)) was computed using the ASGAMAGE temperature and humidity data and their fluxes as discussed in Oost et al. (2000). The accuracy of these has been discussed extensively in that paper and here we only state that the values we will use are a weighted average of the readings of various instruments, with the weight of the data from a sensor taken proportional to the estimated accuracy of the sensor. The estimates of these accuracies are based on a comparison of the heat and humidity data from the various sensors, which functioned independently and had been independently calibrated. The final error in our air temperature is estimated as less than 0.1 °C for most runs, for the water temperature less than 0.05 °C. The average value of the standard deviation between data from the two most important humidity sensors ($\sqrt{2}/2$ times the difference of their readings) was 0.2×10^{-3} kg m^{-3}. These accuracies are amply sufficient for the calculation of the Obukhov length.

Wave measurements were made with a directional waverider, a non-directional waverider and a wave-wire. The data of the last two instruments was combined to get the wave frequency spectrum from low frequencies up to 10 Hz. The smoothness of their merger also gave a check on the performance of these instruments. We converted the directional wave data into information about the presence or absence and the direction(s) of swell using a spectral partitioning method developed by Voorrips et al. (1997), based on ‘inverse catchment’.

Another environmental factor we had to take into account is rainfall. Conventional raingauges do not function properly on our platform, due to its complicated topside, whereas other commercially available rain detectors, based on the conductivity of rain water, easily got saturated and kept indicating rain for some time after it had stopped raining, as we found in a number of tests. We therefore used a meter of our own design, based on the acoustic detection of the impact of rain droplets on a glass sphere as an indicator for rain. Deterioration of the signal due to the sound of the wind blowing along this sphere was avoided by the use of a band pass filter outside the range of the aeolian sounds. This instrument had no delays and a large dynamical range, but we had no possibility for calibration. Below we will discuss the way we used it as an indicator to divide the data into runs with and without rain.

3.2. Data consistency and disturbing effects

3.2.1. *Data Selection and Combination of the A- and B-Periods*

To compare the data sets from the two periods we have plotted u_* as a function of U_{N10} for the A-period in Figure 2a and for the B-period in Figure 2b. We have identified a number of outliers using the Chauvenet criterion (Chauvenet, 1908), which states that data points deviating more than a certain amount from an average value should be omitted from the calculation of those averages and the related standard deviations because they would have a disproportionately large effect on these quantities (rare events). The criterion is based on a normal distribution of the data and can also be applied to the deviation of data from regression lines.

The outliers found with the Chauvenet criterion have been inspected carefully. In most cases we could identify specific conditions such as malfunctioning of instruments, calibration errors or a wind direction that led to significant flow distortion, which confirmed the correctness of the omission of these data from further treatment. In a few cases (15 in all) we could not detect anything special. We have nevertheless omitted these data points from our analysis, assuming that they were either the ‘rare events’ of the Chauvenet criterion or the consequence of some unnoticed and hard to trace malfunction. We have discussed the application of the Chauvenet criterion more extensively in Oost et al. (2000).

To compare the data sets from the A- and the B-periods we made a second-order polynomial fit to u_* as a function of U_{N10} for the A-period (Figure 2a) and plotted the fit on top of the B-data (Figure 2b). For reasons to be given below we have extrapolated this fit to wind speeds beyond the maximum value met during the A-period in this latter figure i.e., outside the range for which the fit was made. For the wind speed range 5–12 m s^{-1}, where we have data from both periods, we see an excellent correspondence that allows us to combine the A- and B-data with confidence and treat them as a single set. When we applied the fit to the data

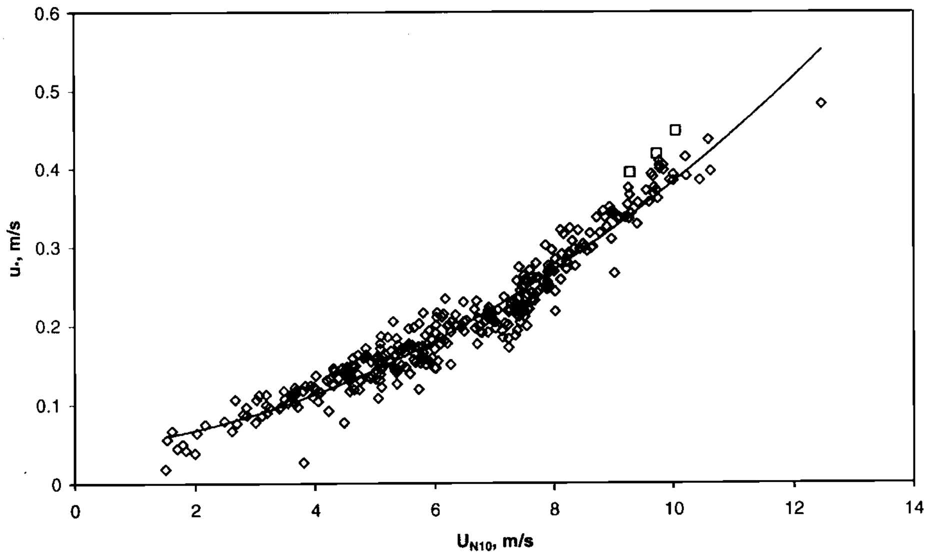

Figure 2a. Friction velocity u_* as a function of the 10 m neutral wind speed U_{N10} for the ASGAMAGE-A period. Diamonds: Accepted data; squares: Suspect data. The curve is a quadratic fit to the accepted data points.

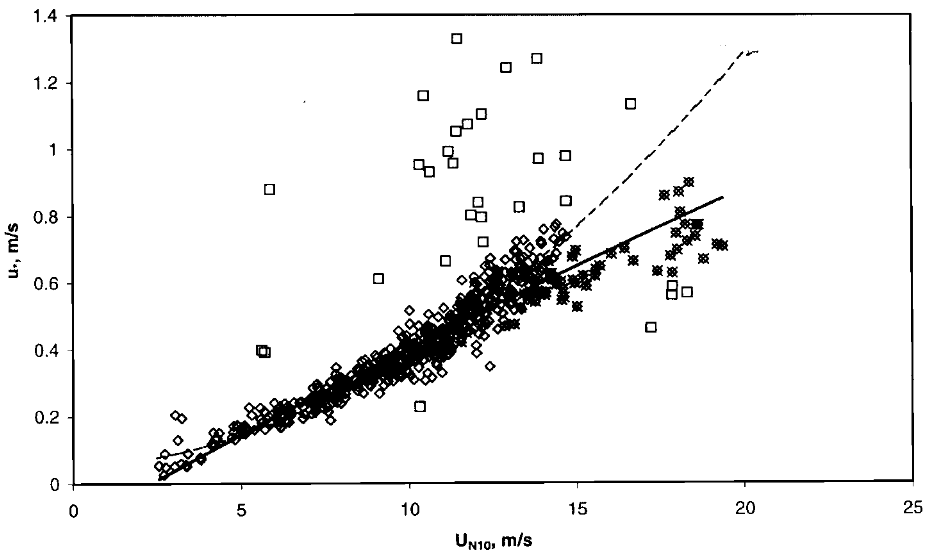

Figure 2b. Friction velocity u_* as a function of the 10-m neutral wind speed U_{N10} for the ASGAMAGE-B period. Diamonds: Accepted data; squares: Suspect data; $\times$: Data from rainy periods. The solid line is a quadratic fit to the accepted data points, the dashed line is the curve of Figure 2a.

of the A-period to the accepted (see below for the meaning of this word in the present paper) data of the B-period we found a residual error of 0.411, whereas the residual error of these B-data for a fit to themselves was 0.407. The minute difference between these two values shows that both data sets are in agreement over the full wind speed range.

3.2.2. *The Effect of 'Rain'*

We noted in Figure 2b that data points beyond about 15 m s^{-1} were more scattered than those below that value and that the trend in that range was different from the one at lower wind speeds. When we plotted the fit to the A-data of Figure 2a in Figure 2b and extrapolated it to U_{N10} = 15 m s^{-1} we noted a bifurcation beyond about 14 m s^{-1}: Part of the B-data are close to the curve for the A-period, the other data show lower u_* values. Beyond 15 m s^{-1} we only find data in the lower branch, there are no data in the upper one. This situation suggests the existence of two different regimes and the most probable cause turned out to be the presence or absence of 'rain'.

To arrive at this conclusion we first had to give a meaning to the readings of our so far uncalibrated rain detector. To this end we took the differences du_* between a fit of u_* as a function of U_{N10} for the combined A and B data sets and the data points and plotted it as a function of the readings of the rain detector (Figure 3). A second-order polynomial fit gave a correlation $R^2 = 0.52$. Based on this fit and the standard deviation of the data at the left side of the plot ($\sigma = 0.034$ for 'rain' < 18000) we chose 'rain' = 18000 as a criterion to distinguish situations with 'rain' from those without it.

When the A and B data were combined all data points beyond U_{N10} = 15 m s^{-1} turned out to be in the category 'rain'. If this interpretation is correct then both Figure 2b and Figure 3 suggest that rain smoothes the surface, a conclusion that would be consistent with the experience of e.g., wind surfers. We have no 'rainy runs' below 10 m s^{-1}, but the gradual merging of the u_* values from both types of runs when the wind speed decreases from 15 to 10 m s^{-1} indicates that, assuming this interpretation of the data is correct, the smoothing effect of 'rain' is only noticeable at a sufficiently high wind speed. Restricting the $u_* - U_{N10}$ fit to 'no rain' data raised the correlation from $R^2 = 0.90$ to $R^2 = 0.95$. In view of the limited amount of information on which the interpretation of the rain gauge data is based we will in what follows only use the 'no rain' data, to avoid complicating the issue. It should be noted that an accidental coincidence between the readings of the rain detector and the diminished stress is improbable, because the 'rainy' data are from various different occasions.

We have indicated the data we have omitted with 'rain', the quotation marks indicating that more factors than rain might be involved. Whether or not this is the case is of no importance for our decision not to combine these data with those with lower readings of the rain detector: that decision was based on the homogeneity requirement for our data set.

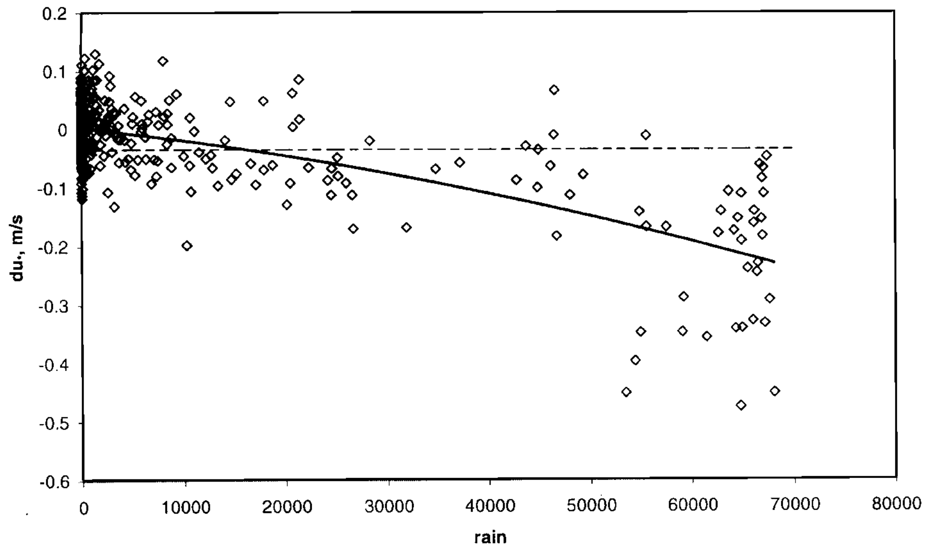

Figure 3. The relation between the signal of the rain detector and the stress. The abscissa gives the reading of the rain detector, on the ordinate the difference between a data point and a quadratic fit to all accepted points is plotted. Solid line: Quadratic fit to the deviations. Dashed line: Standard deviation of the initial data.

3.2.3. *Values of* C_{DN10}

After combining the results from the A and B periods we calculated $C_{DN10} = u_*^2 U_{N10}^{-2}$, the drag coefficient at 10-m height under neutral circumstances, for the accepted data. The result is shown in Figure 4, together with a linear fit and the parameterizations of S80 and Yelland et al. (1998). The regression line

$$C_{DN10} = 1.38 \times 10^{-4} \times U_{N10} + 1.80 \times 10^{-4}$$

gives an acceptable fit to the data ($R^2 = 0.62$), but the data contain a suggestion of a deviation from a linear dependence (the data points at the lower and upper end of the range are mainly above, those in the middle in general below the trendline) and for most wind speeds the MPN data are again significantly higher than those from the open ocean. The fact that the drag coefficient appears not to be a linear function of U_{N10} is more or less as expected in view of the quadratic relationship between u_* and U_{N10}, but for the level of the data we have some explaining to do.

First we checked whether the difference with the open ocean data could be attributed to the specific circumstances of the experiment. We therefore looked into disturbing effects that might have affected our data, viz. flow distortion, tidal currents, distortion of the wave field and the limited water depth.

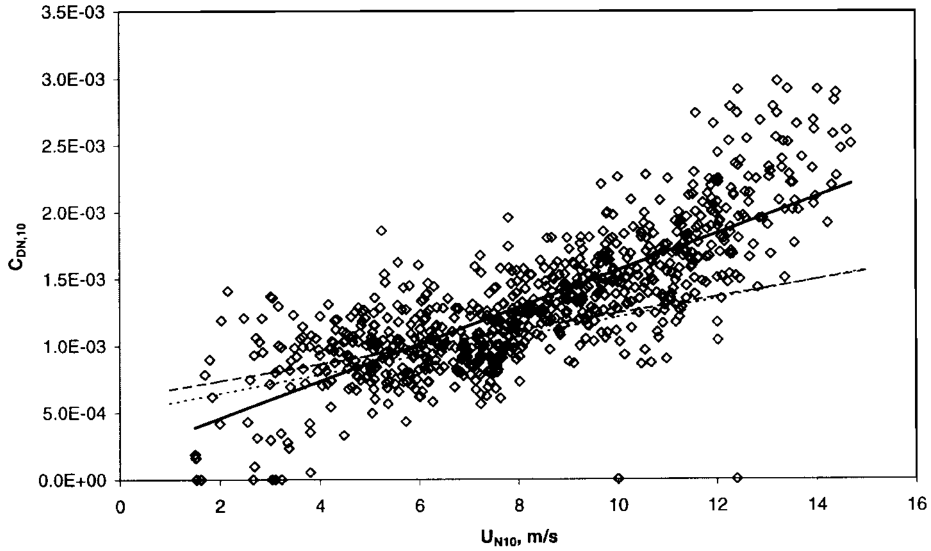

Figure 4. 10-m neutral drag coefficient C_{DN10} as a function of 10-m neutral wind speed U_{N10} for all accepted data. Solid line: Linear fit to the ASGAMAGE data set. Long dashes: S80 parameterization. Short dashes: Parameterization of Yelland et al. (1998).

3.2.4. *Flow Distortion Effects on* u_*

The use of a sizable platform for flux measurements makes extensive precautions necessary to prevent as much as possible flow distortion from affecting the measurements and to correct the remaining effects. Such measures were taken at MPN on the occasion of the HEXMAX experiment and have been maintained since. A 'hardware measure' is the use of the 21-m boom on the west side of the platform at the end of which the flux instruments are mounted to perform these measurements outside the range of strong flow distortion effects. In Oost et al. (1994) the remaining disturbances were discussed and corrections were derived and applied for the mean flow. Based on a wind-tunnel study by Britter et al. (1979) and the dimensions of MPN it was also argued in that paper that no flow distortion correction was needed for turbulent quantities such as u_*. As a check on that supposition we have plotted in Figure 5 the difference between the measured C_{DN10} and a C_{DN10} value based on the u_*/U_{N10} relationship of Figure 2b, together with curves corresponding to plus or minus the standard deviation and the zero line as a function of wind direction. Any flow distortion effect on C_{DN10} (or u_*) should change with wind direction, especially because of the asymmetrical position of the boom with respect to the platform (see Figure 1). We see that the deviations are not significant; particularly gratifying is their tiny value in the south-westerly direction, from which the wind was blowing during a large part of our data runs.

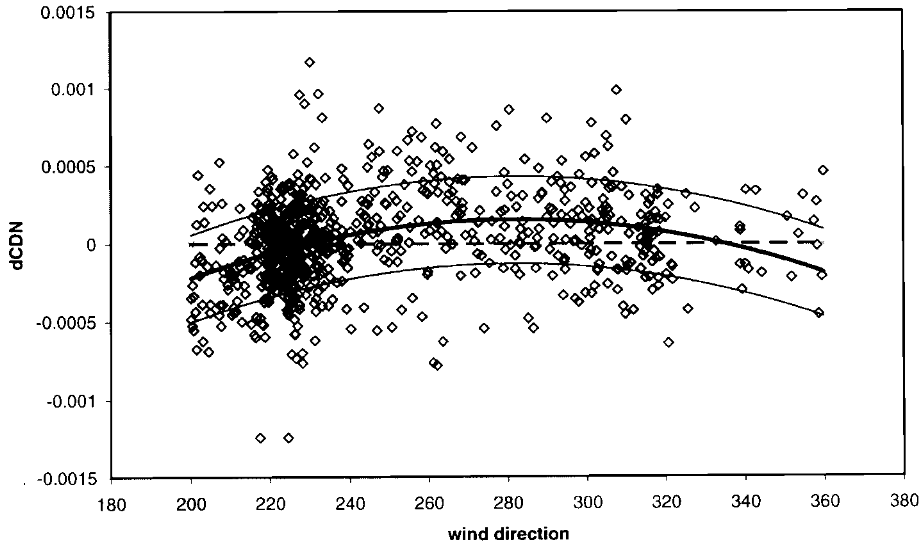

Figure 5. Difference between the actual 10-m neutral drag coefficient C_{DN10} and a parametrized value obtained from a quadratic fit of u_* to U_{N10} as a function of wind direction (degrees from north, starting easterly) with a quadratic regression line (heavy solid line) and error margins at one standard deviation (thin solid lines).

3.2.5. *Effect of Tidal Currents and Distortion of the Wave Field*

MPN is standing in coastal waters, with strong tidal effects, which might have affected the stress data. Although, as already stated, all wind speeds were corrected for the tidal current (not for the wind induced one, to maintain compatibility with data from other areas), there might still be some effects left, e.g., due to non-linear wave-current interactions. We therefore selected from our data a set with negligible currents, plotted the u_* values of this set as a function of U_{N10}, made a fit to these data and compared that fit with two similar ones, one with data from runs with a strong southwest going current and the other with a strong northeasterly current (the tidal ellipse at MPN is fairly narrow, with its main axis in the southwest-northeast direction). The result is shown in Figure 6. The three trend lines are very similar, so we conclude that there are no significant residual effects of the tidal currents on u_*.

MPN (see Figure 1) has a horizontal frame at the water level that might have induced wave reflection and increased breaking. To see whether this frame indeed had any effect on our stress measurements (remember that these were made at the tip of the boom, more than 20 m upwind of the frame just mentioned), we made a division of our stress data in those at low tide, when the frame is above the water level, and data at high tide, when the frame is submerged. If the frame has a measurable effect this should show up in a difference between these two data sets. Figure 7 shows that there is no discernible difference, so we may assume once more that there is no disturbing effect.

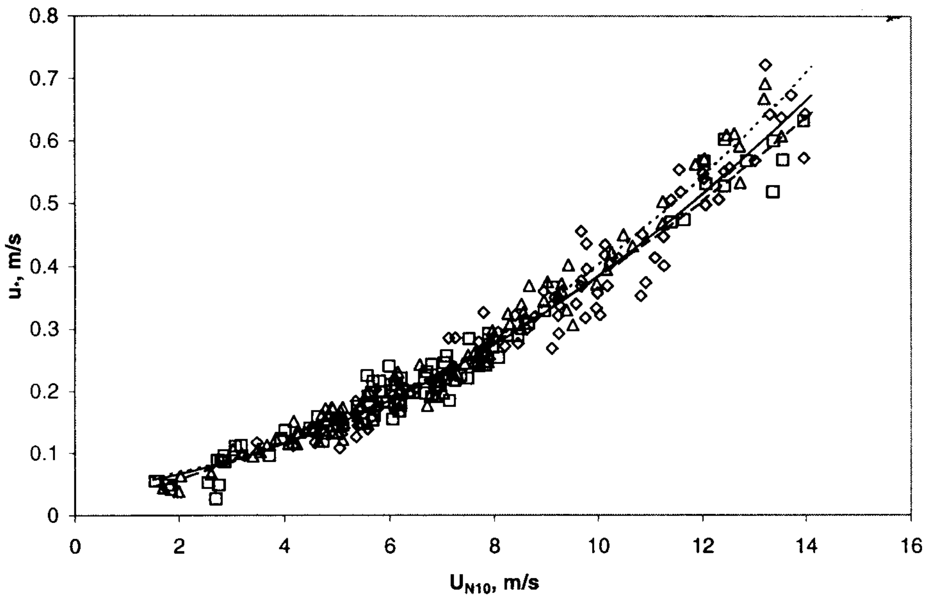

Figure 6. Effect of tide on the friction velocity u_*. Diamonds: runs selected for tidal currents below 0.1 ms^{-1}. Squares: Runs with a strong southwest going current. Triangles: Runs with a strong northeast going current. Solid line: Quadratic fit to data from the periods with a low tidal current. Long dashes: Idem for runs with a strong southwest going current. Short dashes: Idem, for a strong northeast going current.

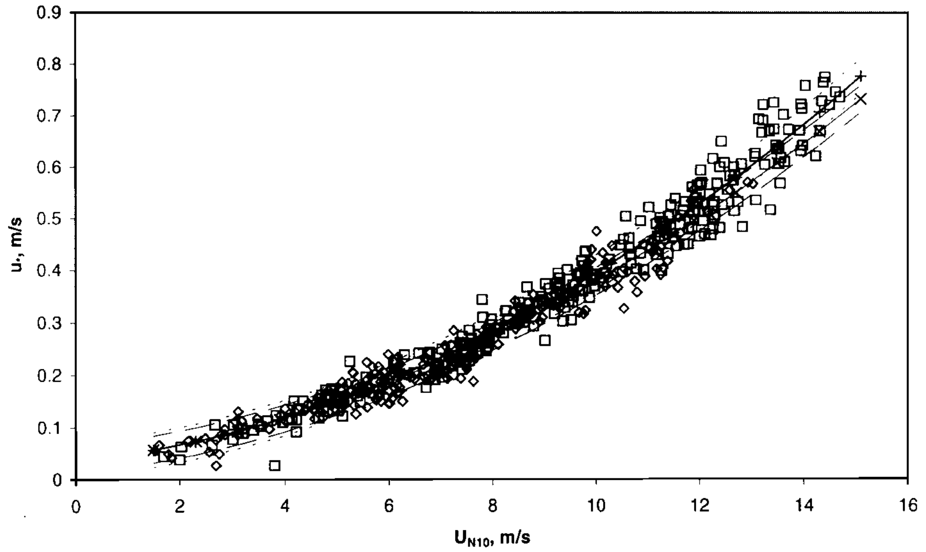

Figure 7. Effect of the horizontal frame at water level of MPN (see Figure 1). Diamonds: Data for low tide situations when the frame was above the water level. Squares: Data taken at high tide with the frame below the water level. Lines are quadratic regression lines (with '+' at high tide and '×' at low tide) and error margins (one standard deviation, long dashes for low tide, short dashes for high tide).

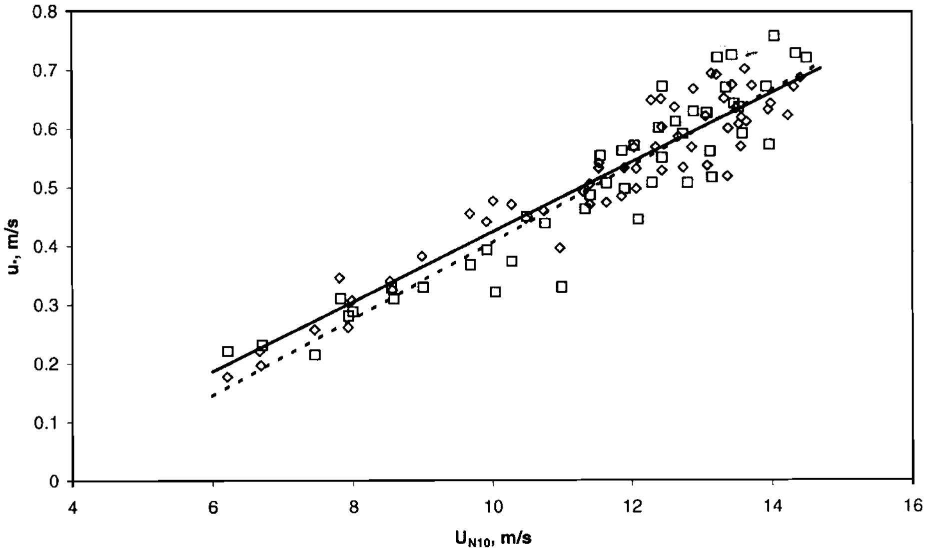

Figure 8. Effect of long wavelengths on the friction velocity u_* as a function of the 10-m neutral wind speed U_{N10}. Diamonds: Runs with wavelengths Λ_p over 80 m. Squares: Runs with wavelengths below 80 m. Both sets have the same wind speed distribution. Lines are linear regression lines, solid for the long wavelength runs, dashed for the other set.

3.2.6. *Limited Water Depth*

In a re-analysis of the HEXMAX data, (Oost, 1998) came to the conclusion that the limited water depth of (on average) 18 m had affected waves with a peak wavelength Λ_p of 80 m and longer: The stress for runs with those wavelengths was systematically higher than the one for runs with shorter peak wavelengths. The wind speed and the wavelength are, however, to some extent correlated, so the effect attributed to the longer waves may just as well have been a consequence of higher wind speeds. To check this we listed all runs in increasing order of wind speed, selected all runs with $\Lambda_p > 80$ m as our first data set and all runs in the list with $\Lambda_p < 80$ m subsequent to one with $\Lambda_p > 80$ m for our second set. In this way the two data sets had the same wind speed distribution (the differences in wind speed for subsequent data points are in the order of only a few tens of mm s^{-1}), but different wavelengths. In Figure 8 we have plotted u_* versus U_{N10} for both data sets. The trend line for each set is well within the error margin of the other one, so there are no grounds to distinguish between situations with peak wavelengths longer or shorter than 80 m.

In conclusion: We find no reason to expect our data to differ from those measured in the open ocean – unless the stress is affected by the properties of the underlying wave field (excluding, based on Figure 8, even a simple relation with the peak wavelength), especially its state of development, which is in general considered to be characterized by the wave age ξ. Some researchers doubt that this is the case (Yelland and Taylor, 1996; Yelland et al., 1998), on the basis of data from the Southern Ocean. In a more theoretical way this stance could be defended from the point of view that the stress is primarily supported by the very short waves, which are always in an approximate equilibrium with the wind. So we will now start looking for surface wave related effects on the stress in our data. As indicated before we will use in what follows the S80 values as our comparison set for the open ocean. We want to stress in this connection that all our considerations and conclusions only apply to the wind speed range covered by our data.

4. The Momentum Flux, the Wind Speed and the Wave Field

4.1. Optimal wind speed level

When we combined the data of the A- and B-periods we found a quadratic dependence for u_* as a function of U_{N10} with a value of 0.95 for the squared correlation R^2. At a single glance it is clear from Figures 2a and 2b that this relationship is indeed not linear. (As an aside we note that neither a linear nor a quadratic relationship between u_* and U_{N10} allows a linear one between C_{DN10} and U_{N10}). The quadratic behaviour is surprising because u_* and U_{N10} both have the dimension of a speed.

Attempts to make them dimensionless with the help of wave field related quantities failed, e.g., when we plotted $u_*(gT_p)^{-1}$ as a function of $U^2_{N10}(gH_s)^{-1}$ (with T_p the peak wave period and H_s the significant wave height) the result was a fan of data points that indeed, with a lot of good will, could be interpreted as a linear relationship, but then a very vague one with $R^2 = 0.17$ and far more scatter than a straightforward u_* vs. U_{N10} plot. We therefore rejected solving the problem by non-dimensionalisation with these wave field related parameters.

It is only an operational convention without any physical underpinning that we customarily use the wind speed at a fixed height of 10 m. The use of such a fixed height is not obvious in case the stress is affected in one way or another by the structure of the wave field: we would expect to need the wind speed at a level related to the wave field. Donelan (1990) suggested the use of a height $\Lambda_p/2$ with Λ_p the wavelength of the peak of the spectrum. He considered the wind speed at that level as an acceptable approximation to U_∞ and used it to bring laboratory and field data closer together. From his figures it is clear that the $U(\Lambda_p/2)$ values are indeed somewhat closer to each other than those at 10m, but they remain distinct (this may – at least partially – be due to the fact that the wind profile in a wave flume is not logarithmic, Oost 1991). Figure 9a depicts u_* as a function of $U(\Lambda_p/2)$ for the ASGAMAGE data. The curvature of the data set is strongly reduced compared to the one in Figures 2a and 2b. A *linear* fit now gives $R^2 = 0.94$, only slightly below the 0.95 for the *quadratic* fit to U_{N10} for the combined data set. The situation improved further when we used the wind speed reduced to neutral circumstances $U_N(\Lambda_p/2)$, resulting in $R^2 = 0.95$, again for a linear fit, and the linear correlation became better once more ($R^2 = 0.96$) when we used $U_N(\Lambda_p)$ instead of $U_N(\Lambda_p/2)$.

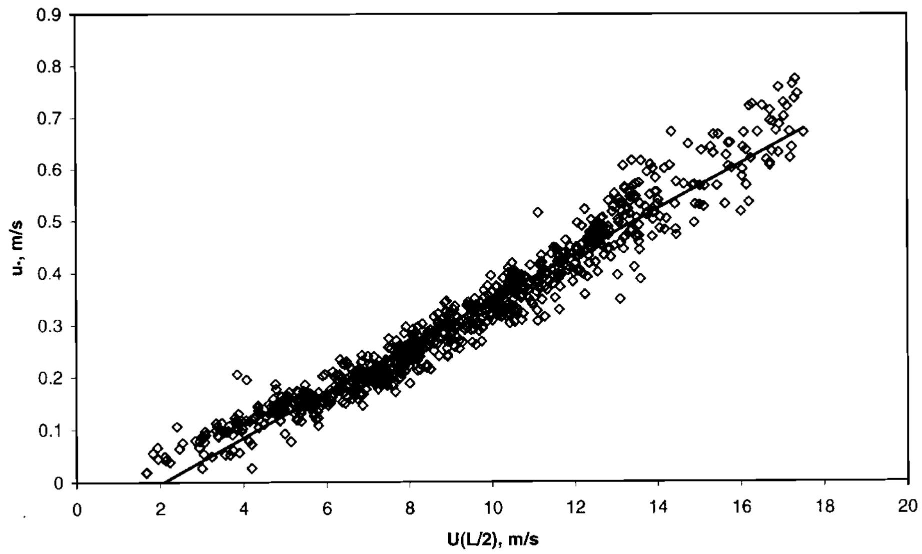

Figure 9a. Friction velocity u_* as a function of the wind speed at a height corresponding to half a peak wavelength. All accepted data. The line is a linear regression line.

These results comprise both runs with only wind sea and runs with swell present. When we restricted our calculations to runs with only wind sea we found even a further improvement. Finally we limited ourselves to wind speeds higher than 6 m s^{-1}, to avoid wind speed ranges where the flow cannot yet be characterized as fully rough. The result of these exercises is shown in Figure 9b and we see that the stress is now a linear and increasing function of the wind speed with $R^2 = 0.964$. A problem is, of course, that peak wavelengths are often so large that the related wind speed level is well outside the constant flux layer. Our present data suggest that it is sufficient in these cases to use an effective wind speed at that level, independent of the actual one.

4.2. The Charnock Parameter α versus the Wave Age

Wave fields do develop only slowly and the question arises whether our data are sufficient to interpret the complex interplay of processes that determine the vertical transport of momentum to the waves or we would need more information about e.g., the wave history for our analysis.

We do not expect this to be really necessary, however. Conservation of momentum requires the turbulent transport in the constant flux layer of the atmosphere to be equal to the momentum flux absorbed by the underlying water surface in a quasi-stationary situation. The ocean/atmosphere system furthermore has two response times: A short one, on the order of (tens of) minutes, in which the atmospheric surface layer adjusts to the wave field, and a long one, on the order of many hours to days, in which the wave field adjusts to a change in the atmospheric

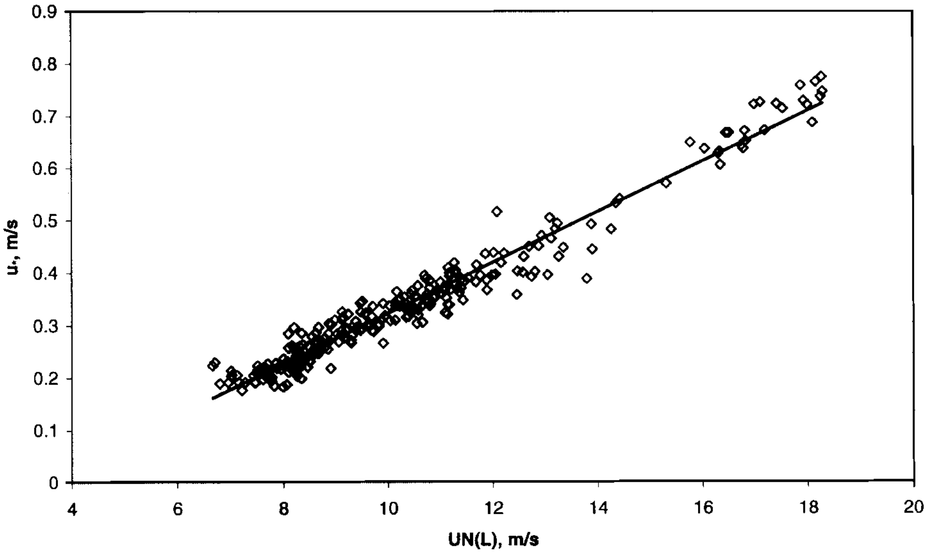

Figure 9b. As Figure 9a, but for the wind speed at a height corresponding to a full peak wavelength and under neutral conditions and for situations with only wind sea and a 10-m wind speed higher than 6 m s^{-1}.

situation. The first one, the fast atmospheric response, allows treating the situation as an equilibrium, despite the slow reactions of the wave field. Therefore we only need the actual conditions, not the history for our analysis.

The values of $\mu = 0.48$ and $n = -1$ in (8), as found in HEXMAX (Smith et al., 1992), hinge on only a few data points. The correlation coefficient R of 0.57 for the linear relationship between $\ln(\alpha)$ and $\ln(\xi)$ for the HEXMAX data is furthermore slightly flattered, because u_* figures in the calculation of both α and ξ, so there is some self-correlation present. In Figure 10 we have plotted $\ln(\alpha)$ versus $\ln(\xi)$ for the ASGAMAGE data (diamonds), a linear fit to these data (solid line), together with lines at one standard deviation (short dashes), the KNMI HEXMAX data and a fit to these data as given in Smith et al. (1992) (long dashes). We remind the reader that we have limited ourselves to runs with 10-m wind speeds $U_{N10} > 6$ m s^{-1} to avoid complications due to low Reynolds number effects. For this figure we have used only runs with (almost) exclusively wind sea, as was done for HEXMAX. For that selection we used a computer programme developed by Voorrips et al. (1997), in which the directional wave spectrum was split in partitions, according to the peaks in that spectrum ('inverse catchment'). We applied three criteria to define wind sea situations: (i) almost all the energy (95% or more) had to be in a single partition, (ii) the direction of the wave field of that partition had to be within 30° of the wind direction and (iii) the phase speed of the waves had to be lower than 1.2 times U_{N10} (Donelan and Hui, 1990). All runs that could not be identified in this way as wind sea runs, including those for which we had no directional wave information, were classified as 'swell' and excluded from Figure 10. This selection

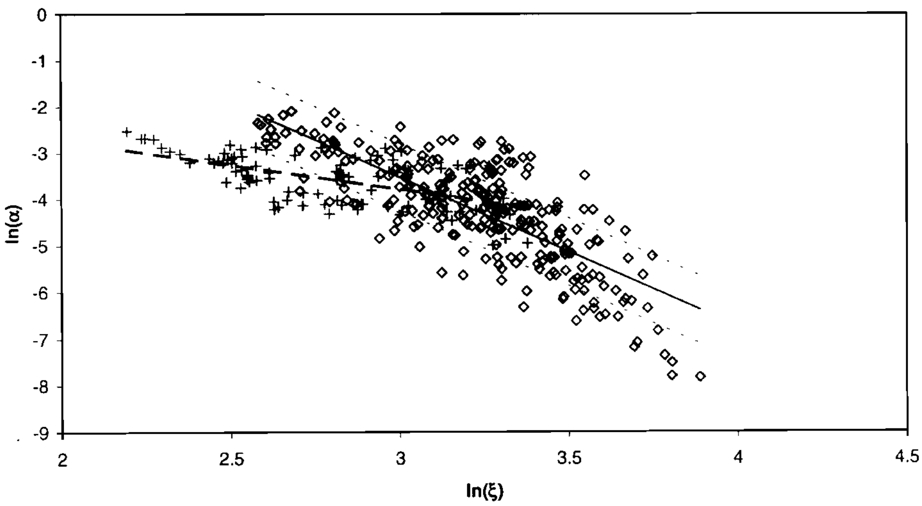

Figure 10. Dimensionless roughness length $\alpha = z_0 g u_*^{-2}$ as a function of the wave age $\xi = c_p u_*^{-1}$ for situations with only wind sea and a 10-m wind speed higher than 6 m s^{-1} for ASGAMAGE (diamonds). Single line: Linear regression line. Short dashes: Lines at one standard deviation from the regression line. For comparison the KNMI HEXMAX data have been added (+). Long dashes: HEXMAX parameterization.

left us with 267 wind sea runs. As with HEXMAX the ASGAMAGE wind sea results show a descending trend when we plot $\ln(\alpha)$ against $\ln(\xi)$:

$$\ln(\alpha) = (-3.21 \pm 0.16) \times \ln(\xi) + (6.11 \pm 0.52) \tag{9a}$$

this time with a correlation coefficient R of 0.78 ($R^2 = 0.60$). The slope ($\mu = -3.21 \pm 0.16$) – as well as the regression coefficient – are much higher than those found with the HEXMAX data (Maat et al., 1991; Smith et al., 1992). The slope is even twice as high as the -1.69 that Monbaliu (1994) found from his analysis of the HEXMAX data set.

The difference between the HEXMAX and ASGAMAGE results might be connected to a difference in the way the distinction between wind sea and swell was made for HEXMAX and the way we have done it here, so we looked more carefully into our selection criteria. We concentrated on the relationship between the wind speed and the phase speed of the (single) peak in the spectrum, the other two criteria being more self-evident. The factor of 1.2 in the phase speed criterion is based on the assumption that in a generating situation the wind speed at 10-m height should not be lower than the phase speed of the waves ($c_p U_{N10}^{-1} < 1$), plus an additional 20% to take care of the fact that the momentum input from the wind to the waves mainly takes place at wavenumbers higher than that of the peak of the spectrum (non-linear interaction then transports the energy to the peak, e.g., Komen et al., 1994, pp. 122–143).

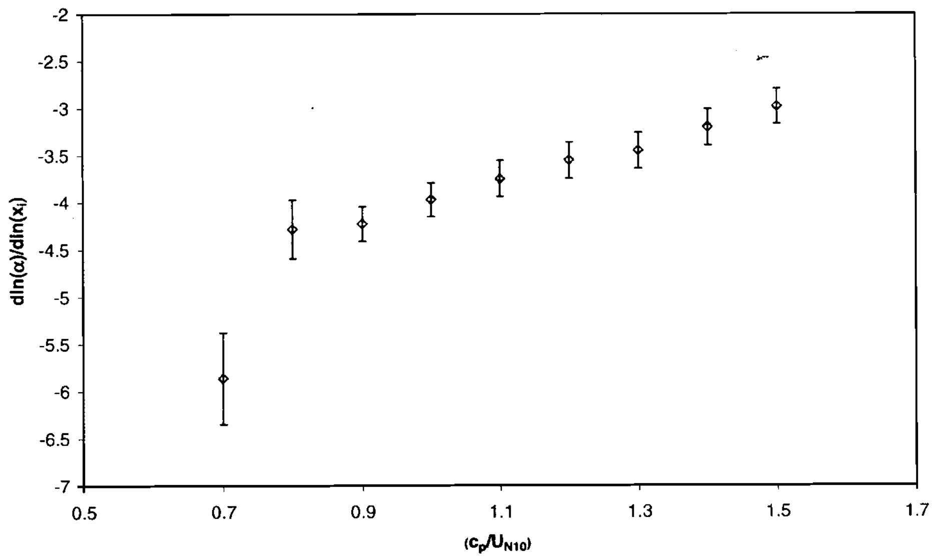

Figure 11. The gradient $\partial \ln(\alpha)/\partial \ln(\xi)$, with α the Charnock parameter and ξ the wave age, $c_p u_*^{-1}$, as a function of the value of $c_p U_{N10}^{-1}$ that is used as upper limit for the indication 'wind sea'.

A measurement height of 10 m has no special properties, as stated earlier, so the factor 1.2 is just as arbitrary. We therefore made a number of calculations in which we decreased the upper limit of the $c_p U_{N10}^{-1}$ ratio from 1.5 to 0.7 in steps of 0.1, hoping to find a value below which the characteristics of the interaction remained constant, allowing us to distinguish between wind sea and swell. The characteristic we used for this purpose was the averaged slope $\partial \ln(\alpha)/\partial \ln(\xi)$. The result is shown in Figure 11. We see that there is a constant increase (in absolute value) of the slope when we reduce the upper limit of the $c_p U_{N10}^{-1}$ range and that the figure shows no plateau. In view of our findings concerning the optimal level for the wind speed we repeated this exercise with $U_N(\Lambda_p)$ instead of U_{N10}, but the result remained roughly the same: A more or less constant change when the upper limit of the $c_p U^{-1}$ range went from 1.5 to 0.8, followed by a steeper part (with U_{N10} there is only a single data point in this last part, with $U_N(\Lambda)$, two). We have to conclude that a $c_p U^{-1}$ criterion does not provide a useful distinction between swell and wind sea.

A problem with the type of fit of Figure 10 is that the outcome is sensitive to the accidental distribution of the data, with ranges with few data getting less weight than those with many data. To see whether this has an important effect in our case we made wave age bins of 0.1, calculated averages and standard deviations for each bin and plotted the result in Figure 12. The differences with Figure 10 are quite noticeable. The most striking one is that up to $\ln(\xi) \approx 3.3$ the data points are

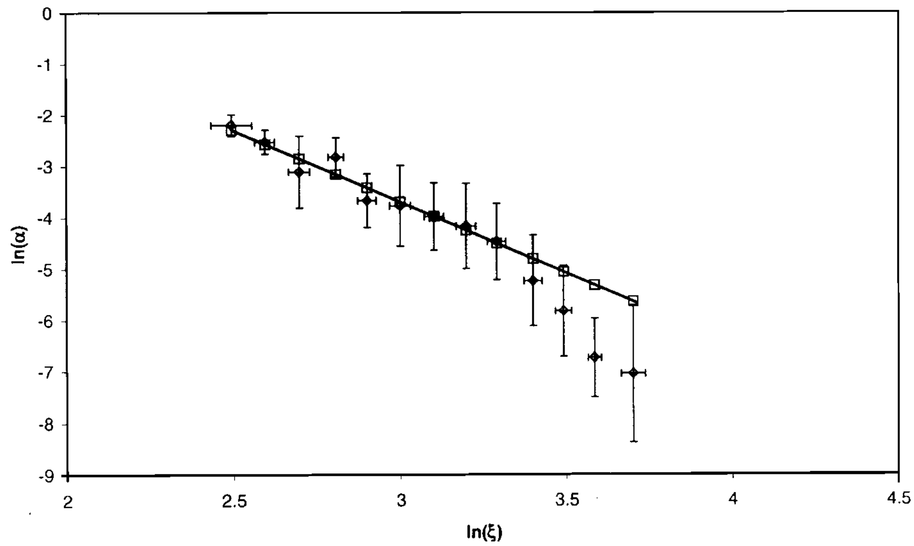

Figure 12. The Charnock parameter $\alpha = z_0 g u_*^{-2}$ as a function of wave age $\xi = c_p u_*^{-1}$ for situations with only wind sea and a 10-m wind speed higher than 6 m s^{-1}, using wave age bins of 0.1. Solid line: Linear regression line for the range $\ln(c_p u_*^{-1}) < 3.3$ (or $c_p u_*^{-1} < 28$).

now very close to a straight line: A regression calculation over this range, giving equal weight to all (averaged) data points, gave

$$\ln(\alpha) = (-2.78 \pm 0.25) \times \ln(\xi) + (4.64 \pm 0.73)$$

with a correlation coefficient $R^2 = 0.95$. The value of 3.3 is in close accordance with a different criterion that is being used for the distinction between wind sea and swell viz. $\xi < 28$ or $\ln(\xi) < 3.33$. Beyond $\ln(\xi) = 3.3$ the data start deviating from a straight line, although they are still within the range $c_p U_{N10}^{-1} < 1.2$. So the $\xi < 28$ criterion is superior to the wind speed related one for the distinction between wind sea and swell (keeping in mind that the data also have to fulfill the criteria for single peakedness and direction). In consequence we repeated our calculation applying the ξ criterion only and found a regression equation

$$\ln(\alpha) = (-2.93 \pm 0.09) \times \ln(\xi) + (5.06 \pm 0.27) \tag{9b}$$

for data that were binned as before (be it with slightly different boundaries of the bins), with a correlation coefficient $R^2 = 0.99$. We consider (9b) as the optimal relationship between wave age and Charnock parameter for wind sea, as far as the ASGAMAGE data are concerned.

There has been some discussion about the effect of the internal accuracy (i.e., the accuracy of the individual data points) on the reliability of a parameterization, which, as in the foregoing, is straightforwardly based on the full data set. Janssen

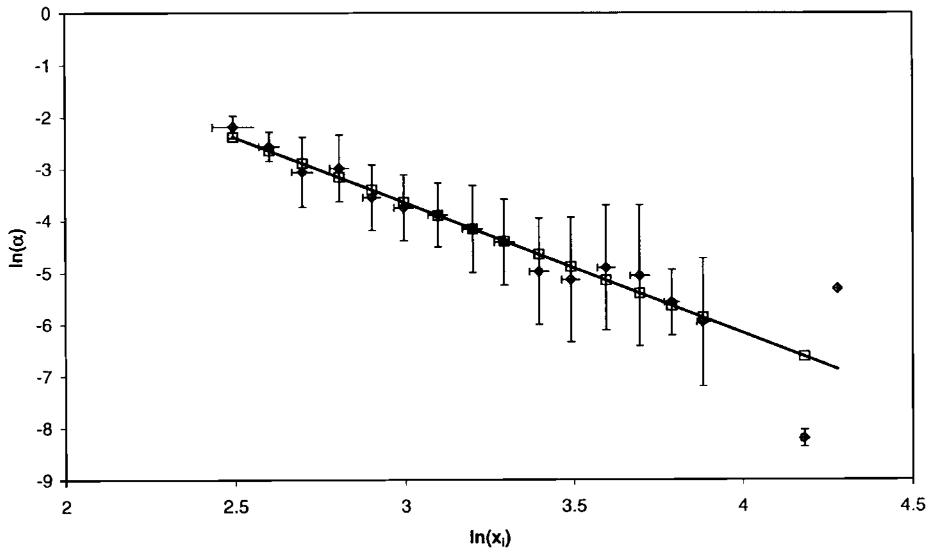

Figure 13. As Figure 12, but for situations with wind sea and swell and a linear regression line for the range $\ln(c_p u_*^{-1}) < 4$ (solid line).

(1997) and Bonekamp et al. (2002) made critical assessments of the validity of various parameterizations, based on estimates of that internal accuracy. We note in this respect that the internal accuracy is a contribution to the total precision that determines the spread of the data around a fitted curve. When the overall accuracy for the full data set is sufficient to draw a conclusion about a parameterization, the accuracy of the individual data points has to be adequate for the purpose. The low values we find for the overall uncertainty of the coefficients in (9a) therefore already show that the internal accuracy is sufficient to support the notion of a wave age dependent α. The accuracy of plus or minus 5% which we finally derived for the slope in a $\ln(\alpha)$ vs. $\ln(\xi)$ plot (see below) furthermore leaves little room for a constant α.

An important asset of ASGAMAGE, compared with other flux studies, is the availability of the detailed wave measurements that allowed us to make a distinction between wind waves and swell. Most other studies did not have comparable information, so, if we want to compare our results with those of others researchers we will have to find the equivalent of (9b) for all situations, independent of the presence or absence of swell. Therefore we repeated the foregoing exercise for all accepted data with $U_{N10} > 6$ m s^{-1}; the result is shown in Figure 13. The slope is slightly less than for the cases of wind sea only. The regression line for this general case is

$$\ln(\alpha) = (-2.52 \pm 0.12) \times \ln(\xi) + (3.91 \pm 0.38) \tag{9c}$$

with R^2 = 0.84. In what follows we will not make a distinction between wind sea and swell anymore.

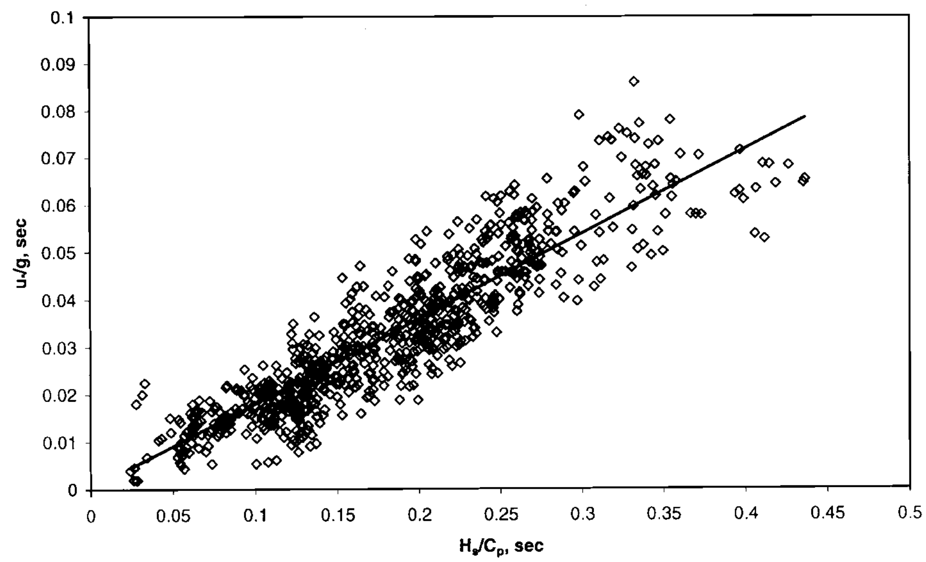

Figure 14. $u_* g^{-1}$ as a function of $H_s c_p^{-1}$ for all accepted runs. The friction velocity u_* is expressed in m s^{-1}, the acceleration of gravity g in m s^{-2}, the significant wave height H_s in m and the phase velocity at the peak of the spectrum c_p in m s^{-1}. The resulting unit on both axes of the figure is therefore seconds.

4.3. Wave age or steepness?

Relation (9c) still suffers from self-correlation. We therefore want to find independent physical properties affecting more directly and instantaneously the air-sea momentum exchange. We started by studying the correlation between $u_* g^{-1}$ on one hand and a steepness related quantity, $H_s c_p^{-1}$ on the other. These combinations are not dimensionless, but all quantities involved are considered to be fully independent, so there is no self-correlation involved; u_* furthermore is a purely atmospheric quantity and H_s and c_p are properties of the wave field. The relationship has the dimension 'time' and the regression line crosses the abscissa very close to the origin, so we can take the regression line through the origin. The correlation is high: $R^2 = 0.82$. The data plot and a linear regression line

$$\frac{u_*}{g} = 0.180 \frac{H_s}{c_p} \tag{10}$$

through the origin are presented in Figure 14. Dividing (10) by c_p and using the deep water dispersion relation

$$\Lambda_p = 2\pi c_p^2 / g \tag{11}$$

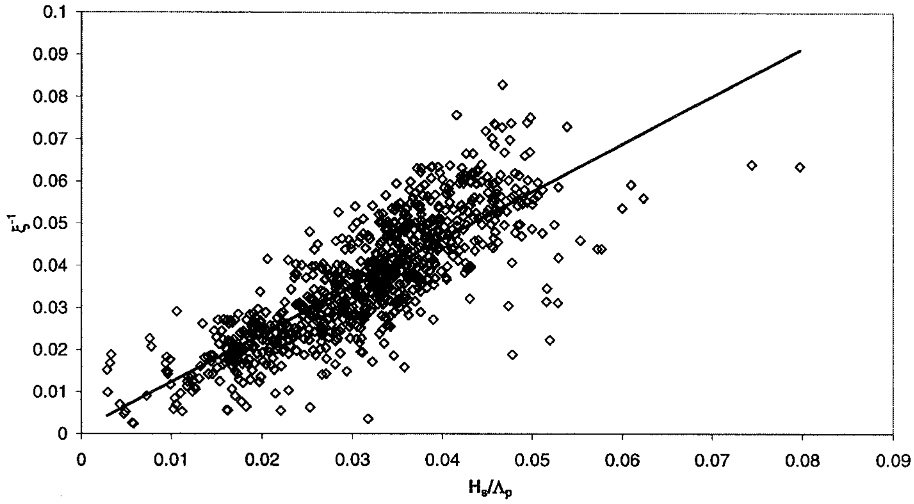

Figure 15. Wave age $\xi = u_* c_p^{-1}$ as a function of the overall wave steepness $H_s \Lambda_p^{-1}$ for situations with wind sea and swell and a 10-m wind speed higher than 6 m s^{-1}.

we find a dimensionless equation relating the (inverse) wave age to the steepness $H_s \Lambda_p^{-1}$:

$$\xi^{-1} = 2\pi \times 0.180 \times \frac{H_s}{\Lambda_p} = 1.13 \times \frac{H_s}{\Lambda_p} \tag{12}$$

We have plotted ξ^{-1} as a function of $H_s \Lambda_p^{-1}$ in Figure 15 for the data with wind speeds larger than 6 m s^{-1}. The slope of the linear trend line is 1.16, in good agreement with the 1.13 of (12); the tiny difference may be attributed to the fact that we have now used the actual wavelengths, whereas (12) was derived using the deep water dispersion relation (11). According to (12) and (9c) $\ln(\alpha)$ should be a linear function of $\ln(H_s \Lambda_p^{-1})$. This is shown in Figure 16. A linear regression calculation gave

$$\ln(\alpha) = (2.17 \pm 0.16) \ln\left(\frac{H_s}{\Lambda_p}\right) + (3.24 \pm 0.56). \tag{13}$$

The correlation is fairly low: R^2 is only 0.23 or $R = 0.48$, somewhat below the $R = 0.57$ for the correlation between α and the wave age for the HEXMAX data (Maat et al., 1991; Smith et al., 1992). This may well, at least partially, be due to the self-correlation in the wave-age relationship, which we now have avoided.

Taylor and Yelland (2001) suggested on the basis of a number of very diverse data sets that the roughness length itself and not α is related to the steepness:

$$\frac{z_0}{H_s} = A \left(\frac{H_s}{\Lambda}\right)^B . \tag{14}$$

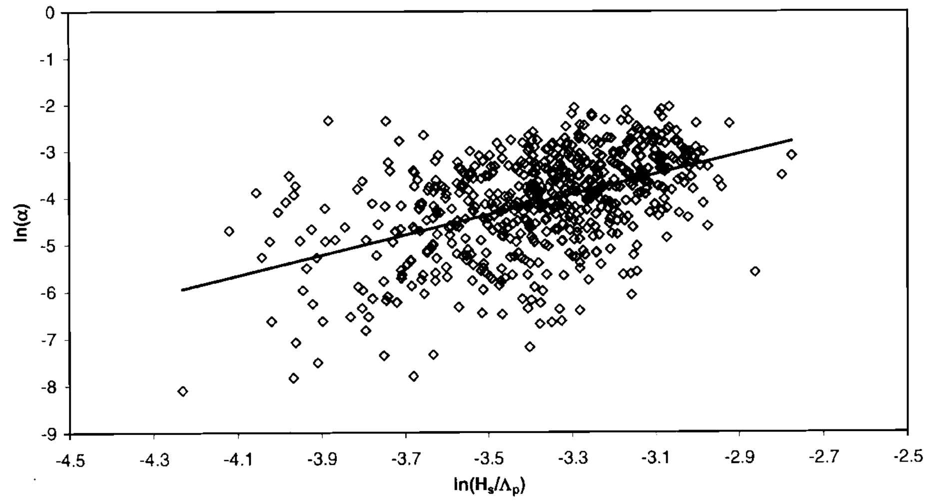

Figure 16. Dimensionless roughness length $\alpha = z_0 g u_*^{-2}$ as a function of the overall wave steepness $H_s \Lambda_p^{-1}$ for situations with only wind sea and a 10-m wind speed higher than 6 m s^{-1}.

When we plotted this relationship we found indeed a connection between this non-dimensionalized roughness length and the steepness. The correlation was rather low again (R^2 = 0.27); the figures we find from a logarithmic fit are A = 4.2, lying with a probability of 68% within the (asymmetric) range 2.1 to 8.5 and B = 3.1 ± 0.2, whereas Taylor and Yelland (2001) suggest A = 1200 and B = 4.5, significantly different from what we found. Their calculations of this relationship could be affected by self-correlation, however, because H_s appears on both sides of the equal sign. To check for this effect we re-arranged the logarithm of (13):

$$\ln(z_0) = \ln(A) + (B+1)\ln(H_s) - B\ln(\Lambda) = \ln(A) + B_1 \ln(H_s) + B_2 \ln(\Lambda) \quad (15)$$

and made a dual regression of $\ln(z_0)$ versus $\ln(H_s)$ and $\ln(\Lambda)$. A crucial test for the single dependence of $z_0 H_s^{-1}$ on the steepness is that $B_1 + B_2$ should be 1. We found $B_1 = 3.83 \pm 0.42$ and $B_2 = -1.57 \pm 0.53$, leading to $B = 2.83 \pm 0.42$ from B_1 and $B = 1.57 \pm 0.53$ from B_2. These two values show a significant difference, so according to the ASGAMAGE data there are other factors affecting z_0, beside the steepness.

4.4. Comparability of MPN and Open Ocean Results

The question is now whether the wave-age (or steepness) dependence we found can explain the difference between the values for the drag coefficient found at MPN and those in the open ocean. To that end we compare the S80 data with the ASGAMAGE values. There is, however, a handicap: S80 only gives wave heights, whereas we need wave ages for this comparison. Fortunately there exists a close relationship between the dimensionless wave height $gH_s u_*^{-2}$ and the wave age (e.g., Maat et al., 1991). Komen et al. (1994) quantify it in their Equations 2.226e, f as

$$\ln(\xi) = 0.6 \ln\left(\frac{gH_s}{u_*^2}\right) - 0.27. \tag{16a}$$

For ASGAMAGE we found

$$\ln(\xi) = 0.65 \ln\left(\frac{gH_s}{u_*^2}\right) - 0.03 \tag{16b}$$

with a correlation $R^2 = 0.87$.

From the wave-height and stress data we derived wave ages with both (16a) and (16b) for the S80 runs and found an average value of 25 for ξ with (16a) and of 24 with (16b), whereas Gulev and Hasse (1998) in their analysis of Voluntary Observing Ships data for the North Atlantic give an average value of 23 for the area where Smith made his measurements. It therefore appears that (16a) and (16b) are fairly robust and that we can use them with some confidence to calculate wave ages for the S80 runs.

For the actual conversion of wave height and stress values of the S80 data into wave ages we have used (16a), because it is based on a much larger and more varied data set than (16b) ((16b) gave comparable results). The resulting relationship between α and ξ is plotted in Figure 17. We see again a wave age dependence of the stress, be it less strong than in ASGAMAGE.

We now want to see whether we can relate the ASGAMAGE results to the S80 conditions. To that end we made a power law fit of the S80 wave ages just calculated to the corresponding U_{10} values

$$\xi = 160.9 U_{10}^{-0.728} \tag{17a}$$

with a correlation $R^2 = 0.31$ (we chose a power law because a linear fit would result in negative wave ages at high wind speeds). A similar fit to the ASGAMAGE data gave

$$\xi = 309.6 U_{10}^{-1.128} \tag{17b}$$

with $R^2 = 0.76$. The ratio of the ξ values calculated with (17a) and (17b) ranges from 1.1 to 1.5 over the wind speed range 7–15 m s^{-1}, so at the same wind speed the waves experienced in S80 are older than those of ASGAMAGE, as should be expected in view of the geographical positions of both platforms.

With (17a) we can calculate the average ξ value to be expected at a certain wind speed at the S80 site off Halifax. From these values we then can determine

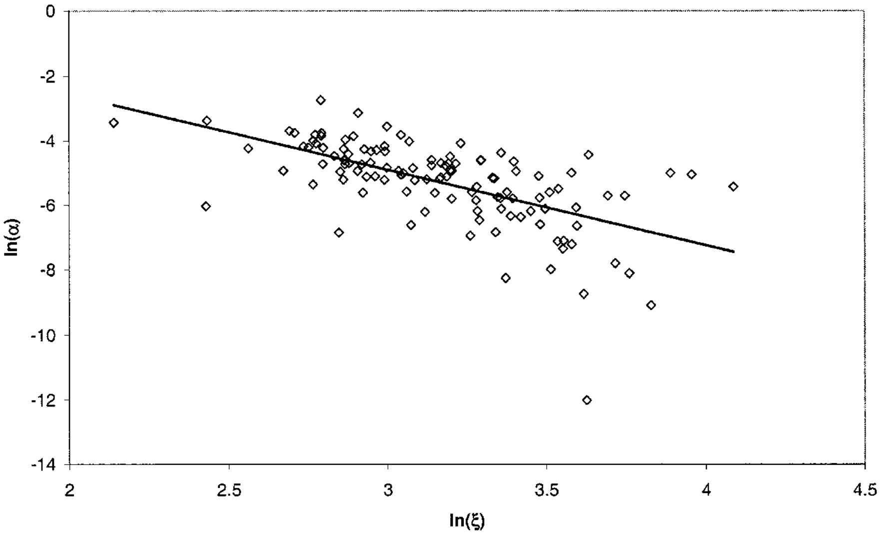

Figure 17. As Figure 10a, but for the data of Smith (1980), after conversion of the development parameter $gH_s u_*^{-2}$ into wave age ξ with Equation (16a).

the corresponding value of α with (9c) and then, from α, u_* and C_{DN10}. The last calculation required an iteration procedure. We did this for wind speeds from 7 to 15 m s^{-1} and the result has been plotted in Figure 18 (crosses). Through the use of (9a) these values can be seen as the ASGAMAGE data, corrected for the wave age difference between MPN and the S80 site and they should be compared to the S80 parameterization, added as the solid line in the graph. The one-sigma deviations (calculated from the figures in S80) are added as dashed lines. The correspondence is as good as may be expected in view of the uncertainties involved. We consider this agreement therefore as a strong indication that the difference between the S80 and ASGAMAGE values for C_{DN10} can be attributed to the difference in wave age at the two sites for the same wind speed and a further proof that the momentum transport at sea is indeed affected by the wave field.

For comparison purposes we have added in Figure 18 the values we find if we calculate C_{DN10} using (17b) instead of (17a) (diamonds). This is actually a fit to the ASGAMAGE data and we have added another fit, based on the quadratic relation between u_* and U_{N10} found earlier (triangles), to show that the rather cumbersome calculation of C_{DN10} with (17b), (9c) and an iteration procedure did not significantly affect the accuracy of the result.

4.5. A WAVELENGTH-RELATED DRAG COEFFICIENT

Equation (9c) provides a relationship between the dimensionless roughness length α and the wave age with which we could transform our North Sea results to those of S80 for the open ocean and which turned out to be independent of the presence

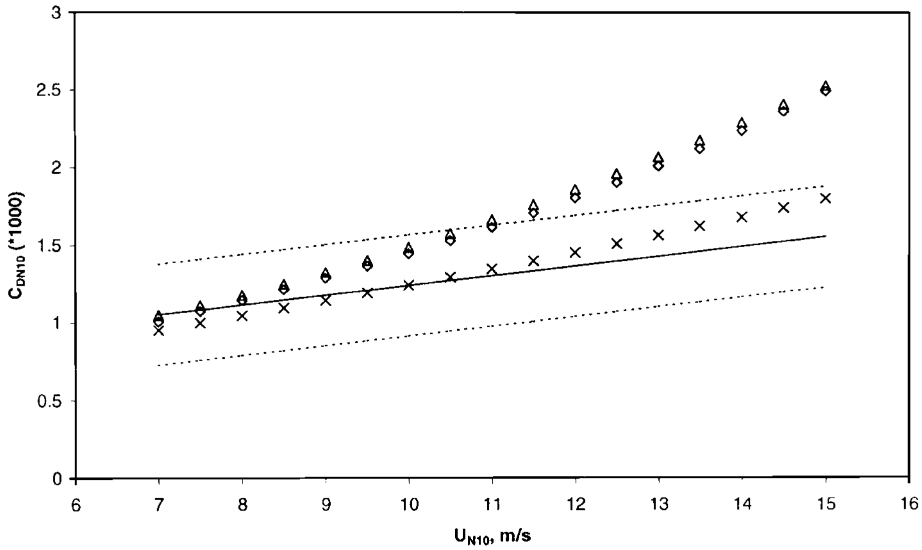

Figure 18. The drag coefficient at 10-m height as a function of 10-m wind speed for neutral circumstances. Triangles: Fit to the ASGAMAGE C_{DN10} data, based on a quadratic relationship between the friction velocity and the 10-m wind speed. Diamonds: Fit to the ASGAMAGE C_{DN10} data based on Equations (9c) and (17b). $\times$: Reduction of the ASGAMAGE C_{DN10} data to the S80 conditions with Equations (9c) and (17a). Solid line: S80 parameterization; the dashed lines indicate the standard deviation of this parameterization.

or absence of swell. This fact points to the general applicability of this relationship, which furthermore implies a stronger wave age dependence than so far surmised. Assuming the general validity of (9c) and combining it with (2), (3) and (11) we find a relationship between the wave age and the (effective) drag coefficient C_{DNL} at a height Λ_p

$$\frac{\kappa}{C_{DNL}^{0.5}} = 4.52\ln(\xi) + \ln(2\pi) - 3.91 = 4.52\ln(\xi) - 2.07. \tag{18}$$

It is a straightforward procedure to calculate e.g., U_{N10} once C_{DNL} and the wavelength are known.

5. Summary and Conclusions

The ASGAMAGE data, like those from 1986 HEXMAX experiment (Maat et al., 1991; Smith et al., 1992), shows a wave age dependent Charnock parameter α. The data show good agreement with those measured during HEXMAX. An important difference with the HEXMAX situation is the range of wave ages covered. This has as a consequence that the slope in a logarithmic plot of α against ξ for ASGAMAGE is steeper than the HEXMAX value of -1. The error margin is much lower, excluding far more clearly than in the earlier experiment a constant value for α.

Using an empirically determined relationship between the non-dimensional wave height and the wave age we have estimated wave age values for the S80 runs. For the same wind speed these wave ages turned out to be much higher than those we found in ASGAMAGE. Applying this phenomenon and the connection found between wave age and stress we could explain – to within the accuracy limits of the S80 parameterization – the difference between the C_{DN10} parameterization of S80 and the values for this quantity in ASGAMAGE. We therefore surmise that the existing plethora of relations between the drag coefficient and the wind can largely be attributed to the fact that in most experiments little or no account has been taken of the value of either the steepness or the wave age of the underlying wave field.

This being said the relationship between the Charnock parameter $\alpha(= z_0 g u_*^{-2})$ and the wave age ξ $(= c_p u_*^{-1})$ still is affected by self-correlation (both quantities contain u_*). We therefore used the connection between $u_* g^{-1}$ and $H_s c_p^{-1}$, which does not suffer from self-correlation and has a clear separation between oceanographic and atmospheric quantities. We found a close proportionality that allowed us to derive a connection between wave age and the steepness $H_s \Lambda_p^{-1}$ of the waves and so, in combination with the foregoing, between the Charnock parameter and the steepness.

The accuracy of our data permits the conclusion that, at least for our experiment, the relationship between u_* and U_{N10} is primarily a quadratic one. This is not only in glaring and irreparable conflict with dimensional considerations, but it also contradicts the often used assumption of a linear dependence of C_{DN10} on U_{N10}. A linear relationship cannot reproduce the connection between u_* and U_{N10} and remain within the error limits over the full wind speed range of our data (the linear term in the full second order fit is by far the smaller one). We did find the expected linear relationship, however, when, in line with earlier work of Donelan (1990), we related u_* to the wind speed at a wavelength related level. $U_N(\Lambda)$ gave in this connection an even better linearity than $U_N(\Lambda/2)$, proposed by Donelan (1990). Good relationships, i.e., close to linear, also resulted when we used the (effective logarithmic) wind at larger heights, e.g., 100 m or beyond, by extrapolating the logarithmic profile to that level. This latter effect must, however, be considered as not more than a mathematical consequence of the use of a logarithmic wind profile with a fixed friction velocity. For wind speeds of 6 m s^{-1} and higher we did not find large differences between runs with and those without swell waves. Neither did we see an effect of the limited depth at MPN. We could explain the apparent bottom influence surmised by Oost (1998) as an artefact due to the correlation between wind speed and wave height and the non-linear relationship between the stress and the wind speed. We found indications for, but made no further study of, an effect of rain on the stress at high wind speed.

Acknowledgements

We specifically would like to thank Ed Worrell, our technical wizard without whose unceasing activities we wouldn't have had any data to start with, let alone the high quality data that are the backbone of this paper. We have benefited from discussions with Peter Janssen. We thank Hans Bonekamp for running his statistical tests on the ASGAMAGE data and Aart Voorrips for providing his spectral partitioning programme.

This research has been undertaken in the framework of the ASGAMAGE project. ASGAMAGE is a contribution to the International Global Atmospheric Chemistry (IGAC) Core Project of the International Geosphere-Biosphere Programme (IGBP) and part of the Marine Aerosol and Gas Exchange (MAGE) Activity. We gratefully acknowledge financial support from the European Commission 's Marine Science and Technology Programme (MAST III) under contract MAS3-CT95-0044.

References

Bonekamp, H., Komen, G. J., Sterl, A., Janssen, P. A. E. M., Taylor, P. K., and Yelland, M. J.: 2002, 'Statistical Comparisons of Observed and ECMWF Modeled Open Ocean Surface Drag', *J. Phys. Oceanog*, in press.

Britter, R. E., Hunt, J. C. R., and Mumford, J. C.: 1979, 'The Distortion of Turbulence by a Circular Cylinder', *J. Fluid Mech.* **92**, 269–301.

Businger, J. A., Wyngaard, J. C., Izumi, Y., and Bradley, E. F.: 1971, 'Flux-profile Relationships in the Atmospheric Surface Layer', *J. Atmos. Sci.* **28**, 181–189.

Charnock, H.: 1955, 'Wind Stress on a Water Surface', *Quart. J. Roy. Meteorol. Soc.* **81**, 639–640.

Chauvenet, W.: 1908, 'A Manual of Spherical and Practical Astronomy', 5th edn., Vol. 2, Lippincott, Philadelphia, 632 pp.

Donelan, M.: 1990, 'Air-Sea Interaction', in B. LeMéhauté and D. M. Hanes (eds.), *The Sea*, Vol. 9A, J. Wiley, New York, pp. 239–292.

Donelan, M. A. and Hui, W. H.: 1990, 'Mechanics of Ocean Surface Waves', in G. L. Geernaert and W. J. Plant (eds.), *Surface Waves and Fluxes*, Vol. 1, Kluwer Academic Publishers, Dordrecht, pp. 209–246.

Donelan, M., Dobson, F. W., Smith, S. D., and Anderson, R. J.: 1993, 'On the Dependence of Sea Surface Roughness on Wave Development', *J. Phys. Oceanog.* **23**, 2143–2149.

Dyer, A. J. and Hicks, B. B.: 1970, 'Flux-Gradient Relationships in the Constant Flux Layer', *Quart. J. Roy. Meteor. Soc.* **96**, 715–721.

Eymard, L., Caniaux, G., Dupuis, H., Prieur, D., Giordani, H., Troadec, R., Bessemoulin, P., Lachaud, G., Bouhours, G., Bourras, D., Guérin, LeBorgne, P., Brisson, A., and Marsouin, A.: 1999, 'Surface Fluxes in the North Atlantic during CATCH/FASTEX', *Quart. J. Roy. Meteor. Soc.* **125**, 3563–3599.

Gerritsen, H., de Vries, J. H., and Philippart, M.: 1995, 'The Dutch Continental Shelf Model', in D. R. Lynch and A. M. Davies (eds.), *Quantitative Skill Assessment for Coastal Ocean Models, Coastal and Estuarine Studies 47*, American Geophysical Union, Washington, DC, 510 pp.

Gulev, S. K. and Hasse, L.: 1998, 'North Atlantic Wind Waves and Wind Stress Fields from Voluntary Observing Ship Data', *J. Phys. Oceanog.* **28**, 1107–1130.

Janssen, J. A. M.: 1997, 'Does Wind Stress Depend on Sea-State or Not? – A Statistical Analysis of HEXMAX Data', *Boundary-Layer Meteorol.* **83**, 479–503.

Komen, G. J., Cavaleri, L., Donelan, M., Hasselmann, K., Hasselmann, S., and Janssen, P. A. E. M.: 1994, *Dynamics and Modelling of Ocean Waves*, Cambridge University Press, Cambridge, 532 pp.

Maat, N., Kraan, C., and Oost, W. A.: 1991, 'The Roughness of Wind Waves', *Boundary-Layer Meteorol.* **54**, 89–103.

Makin, V. K., Kudryavtsev, V. N., and Mastenbroek, C.: 1995, 'Drag of the Sea Surface', *Boundary-Layer Meteorol.* **73**, 159–182.

Monbaliu, J.: 1994, 'On the Use of the Donelan Wave Spectral Parameter as a Measure for the Roughness of Wind Waves', *Boundary-Layer Meteorol.* **67**, 277–291.

Monin, A. S. and Obukhov, A. M.: 1954, 'Basic Laws of Turbulent Mixing in the Surface Layer of the Atmosphere', *Tr. Akad Nauk SSSR, Geofiz. Inst.* **24**, 163–187.

Oost, W. A.: 1991, 'The Wind Profile in a Wave Flume', *J. Wind Engng. Indust. Aerodynam.* **37**, 113–121.

Oost, W. A.: 1998, 'The KNMI HEXMAX Stress Data – A Reanalysis', *Boundary-Layer Meteorol.* **86**, 447–468.

Oost, W. A., Fairall, C. W., Edson, J. B., Smith, S. D., Anderson, R. J., Wills, J. A. B., Katsaros, K. B., and deCosmo, J.: 1994, 'Flow Distortion Calculations and their Application in HEXMAX', *J. Atmos. Oceanic Tech.* **11**, 366–386.

Oost, W. A., Jacobs, C. M. J., and van Oort, C.: 2000, 'Stability Effects on Heat and Moisture Fluxes at Sea', *Boundary-Layer Meteorol.* **95**, 271–302.

Oost, W. A., Worrell, E. H. W., Schaap, J. W., van Oort, C., and Kraan, C.: 1991, 'An Improved Version of the Pressure Anemometer', *J. Atmos. Oceanic Tech.* **8**, 575–584.

Smith, S. D.: 1980, 'Wind Stress and Heat Flux over the Ocean in Gale Force Winds', *J. Phys. Oceanog.* **10**, 709–726.

Smith, S. D., Anderson, R. J., Oost, W. A., Kraan, C., Maat, N., DeCosmo, J., Katsaros, K. B., Davidson, K. L., Bumke, K., Hasse L., and Chadwick, H. M.: 1992, 'Sea Surface Wind Stress and Drag Coefficients: The HEXOS Results', *Boundary-Layer Meteorol.* **60**, 109–142.

Taylor, P. K. and Yelland, M. J., 2001: 'The Dependence of Sea Surface Roughness on the Height and Steepness of the Waves', *J. Phys. Oceanog.* **31**, 572–590.

Yelland, M. and Taylor, P. K.: 1996, 'Wind Stress Measurements from the Open Ocean', *J. Phys. Oceanog.* **26**, 541–558.

Yelland, M. J., Moat, B. I., Taylor, P. K., Pascal, R. W., Hutchings, J., and Cornell, V. C.: 1998, 'Wind Stress Measurements from the Open Ocean Corrected for Air Flow Distortion by the Ship', *J. Phys. Oceanog.* **28**, 1511–1526.

Voorrips, A. C, Makin, V. K., and Hasselmann, S.: 1997, 'Assimilation of Wave Observations from Pitch-and-Roll Buoys in a North Sea Wave Model', *J. Geophys. Res.* **102**, 5829–5849.

Wills, J. A. B.: 1984, *HEXOS Model Tests on the Noordwijk Tower*, Report R. 184, British Maritime Technology Ltd, Teddington, U.K., 56 pp.